ANESTHESIOLOGY

Altered Global Brain Signal during Physiologic, Pharmacologic, and Pathologic States of Unconsciousness in Humans and Rats

Sean Tanabe, B.S., Zirui Huang, Ph.D., Jun Zhang, M.D., Ph.D., Yali Chen, M.D., Stuart Fogel, Ph.D., Julien Doyon, Ph.D., Jinsong Wu, M.D., Ph.D., Jianghui Xu, M.D., Jianfeng Zhang, M.S., Pengmin Qin, Ph.D., Xuehai Wu, M.D., Ph.D., Ying Mao, M.D., Ph.D., George A. Mashour, M.D., Ph.D., Anthony G. Hudetz, D.B.M., Ph.D., Georg Northoff, M.D., Ph.D.

ANESTHESIOLOGY 2020; 132:1392–406

EDITOR'S PERSPECTIVE

What We Already Know about This Topic

- Integrated neuronal activity across functionally distinct brain networks is a prerequisite for consciousness
- Functional magnetic resonance imaging–derived global brain signal is a candidate marker for conscious states
- Whether unconsciousness is correlated with a loss of global temporal coordination of brain activities has not been previously reported

What This Article Tells Us That Is New

- Functional magnetic resonance imaging of global brain signal amplitude and functional connectivity demonstrates a strong association between overall brain connectivity and the level of consciousness in both humans and rats
- Each distinct state of unconsciousness, including sleep, general anesthesia, and unresponsive wakefulness syndrome, showed state-specific alterations in global signal topography
- These findings suggest that the global temporal coordination defines the coarse-grained state of consciousness *versus* unconsciousness, while the relationship of the global and local signals defines the particular qualities of that unconscious state

ABSTRACT

Background: Consciousness is supported by integrated brain activity across widespread functionally segregated networks. The functional magnetic resonance imaging–derived global brain signal is a candidate marker for a conscious state, and thus the authors hypothesized that unconsciousness would be accompanied by a loss of global temporal coordination, with specific patterns of decoupling between local regions and global activity differentiating among various unconscious states.

Methods: Functional magnetic resonance imaging global signals were studied in physiologic, pharmacologic, and pathologic states of unconsciousness in human natural sleep (n = 9), propofol anesthesia (humans, n = 14; male rats, n = 12), and neuropathological patients (n = 21). The global signal amplitude as well as the correlation between global signal and signals of local voxels were quantified. The former reflects the net strength of global temporal coordination, and the latter yields global signal topography.

Results: A profound reduction of global signal amplitude was seen consistently across the various unconscious states: wakefulness (median [1st, 3rd quartile], 0.46 [0.21, 0.50]) *versus* non-rapid eye movement stage 3 of sleep (0.30 [0.24, 0.32]; $P = 0.035$), wakefulness (0.36 [0.31, 0.42]) *versus* general anesthesia (0.25 [0.21, 0.28]; $P = 0.001$), healthy controls (0.30 [0.27, 0.37]) *versus* unresponsive wakefulness syndrome (0.22 [0.15, 0.24]; $P < 0.001$), and low dose (0.07 [0.06, 0.08]) *versus* high dose of propofol (0.04 [0.03, 0.05]; $P = 0.028$) in rats. Furthermore, non-rapid eye movement stage 3 of sleep was characterized by a decoupling of sensory and attention networks from the global network. General anesthesia and unresponsive wakefulness syndrome were characterized by a dissociation of the majority of functional networks from the global network. This decoupling, however, was dominated by distinct neuroanatomic foci (*e.g.*, precuneus and anterior cingulate cortices).

Conclusions: The global temporal coordination of various modules across the brain may distinguish the coarse-grained state of consciousness *versus* unconsciousness, while the relationship between the global and local signals may define the particular qualities of a particular unconscious state.

(ANESTHESIOLOGY 2020; 132:1392–406)

Despite various distinctions among modern theories of consciousness,[1–4] there seems to be a common requirement for a global component that is tightly associated with conscious states, *i.e.*, integrated brain activity across widespread functionally segregated networks. Integrated Information Theory states that consciousness is integrated information, resulting in experience that is both differentiated and integrated.[1] Global Neuronal Workspace Theory argues that conscious access emerges when incoming sensory information is broadcast globally to multiple cognitive

This article is featured in "This Month in Anesthesiology," page 1A. This article has a video abstract. S.T. and Z.H. contributed equally to this article.

Submitted for publication June 27, 2019. Accepted for publication January 16, 2020. Published online first on March 19, 2020. From the Department of Anesthesiology, Huashan Hospital, Fudan University, Shanghai, China (J.Z., Y.C., J.X.); the Department of Anesthesiology and Center for Consciousness Science, University of Michigan, Ann Arbor, Michigan (S.T., Z.H., G.A.M., A.G.H.); Institute of Mental Health Research (S.F., G.N.), School of Psychology (S.F.), University of Ottawa, Ottawa, Canada; Department of Psychology, University of Montreal, Montreal, Canada (S.F., J.D.); Functional Neuroimaging Unit, Institute of Geriatrics, University of Montréal, Montréal, Canada (S.F., J.D.); McConnell Brain Imaging Center, Montreal Neurological Institute, McGill University, Montreal, Canada (J.D.); Department of Neurosurgery, Huashan Hospital, Fudan University, Shanghai, China (J.W., X.W., Y.M.); Mental Health Center, Zhejiang University School of Medicine, Hangzhou, Zhejiang, China (J.Z., G.N.); School of Psychology, South China Normal University, Guangzhou, Guangdong, China (P.Q.).

 Anesthesiology 2020; 132:1392–406. DOI: 10.1097/ALN.0000000000003197

systems allowing information to be flexibly shared across cortical processors.[2,3] Temporospatial Theory of Consciousness emphasizes the central role of temporospatial nestedness of neuronal activity throughout the brain, which enables sensory inputs to be aligned with the ongoing brain activity, expanded, and globalized both in time and space.[4]

The functional magnetic resonance imaging–derived global signal refers to the average time course of brain activity of all gray matter voxels and might be a candidate marker of conscious states.[5–7] The value of the global signal at each time point reflects transient global temporal coordination across voxels at that time.[8–11] When the temporal coordination is high, *i.e.,* most voxels have the same sign (either positive or negative), the summation of the values across voxels will tend to be either positive or negative. On the other hand, when the temporal coordination is low, *i.e.,* the proportions of positive and negative voxel values are roughly equal, the voxel values tend to cancel out and the global signal value will be close to zero. By measuring the amplitude of global signal, referring to the SD of the global signal over the course of the scan, one can infer the net strength of global temporal coordination or overall brain connectivity.[6] Furthermore, the correlation between the global signal and the signals of local voxels reflects how much each voxel's temporal variance is shared with that of the global signal. We defined the resulting spatial map as the global signal representation across the brain—global signal topography.[6,7,12] Despite some controversy about the origin of the global functional magnetic resonance imaging signal, *e.g.,* that it may in part reflect noise,[13] recent empirical and neural modeling studies suggest that the global signal has a physiologic and neural basis.[5,8,9,11,14–23] However, the relevance of the global brain signal in general, and that of the global signal amplitude and global signal topography in particular, to consciousness remains an open question.

To fill this gap of knowledge, we investigated how the global brain signal changes across the spectrum of different states of consciousness. We hypothesized that unconsciousness is accompanied by a loss of global temporal coordination, while specific patterns of decoupling between local regions and global activity may distinguish different kinds of unconscious states. In order to obtain a generally valid answer, we examined functional magnetic resonance imaging–derived global signals across physiologic, pharmacologic, and pathologic states of unconsciousness: different natural sleep stages (non-rapid eye movement stage 1, stage 2, and stage 3) in humans; sedation and general anesthesia in humans and rats; and minimally conscious state and unresponsive wakefulness syndrome in human patients.

Materials and Methods

Human Natural Sleep

The human natural sleep electroencephalography functional magnetic resonance imaging data have been previously published.[24,25] The experiment was approved by the Research Ethics Board at the Institute of Geriatrics, University of Montreal, Montreal, Canada. The study included nine right-handed healthy participants (male/female: 5/4). The original data set included 13 subjects,[25] but 4 subjects were excluded due to insufficient segment size (eliminated segments with fewer than eight time points) for non-rapid eye movement stage 3, leaving 9 subjects for this study. Participants had normal body weight (body mass index 25 or less) and no history of psychiatric or neurologic disorder (see reference 25 for more details of inclusion criteria). At least 7 days before the study, the participants were asked to keep a regular sleep-wake cycle (bedtime 10:00 PM to 1:00 AM, waketime 7:00 AM to 10:00 AM) and avoid taking daytime naps. Adherence to this schedule was confirmed using actigraphy and a sleep diary. All participants underwent an acclimatization night in a mock scanner.

Electroencephalography data were used to determine the sleep stages. The human natural sleep study used a 64-channel magnetic resonance–compatible electroencephalography cap (Braincap MR, Easycap, Germany). Data were recorded at 5,000 samples/s with 500-nV resolution and filtered to 0.016 to 250 Hz. Data were transferred and synchronized to a scanner clock using Brain Products Recording Software, Version 1.x (Brain Products, Germany). The electroencephalography data were sleep stage–scored using standard American Academy of Sleep Medicine (Darien, Illinois) criteria after preprocessing by removing gradient artifacts using adaptive average subtraction and correcting ballistocadiographic artifacts using a combination of artifact template subtraction and event-related independent component analysis using the "fMRI Artifact Rejection and Sleep Scoring Toolbox." Data were then low-pass filtered at 60 Hz, down-sampled to 250 samples/second, and rereferenced to average mastoids.

All human natural sleep functional magnetic resonance imaging data were acquired by 3T Siemens Trio Total imaging matrix systems (Siemens, Germany) with a 12-channel head coil. The echo-planar images were acquired at repetition-time/echo-time = 2,160/30 ms, slice thickness = 3 mm, number of slices = 40, field of view = 220 mm, flip angle = 90°, and matrix size = 64 × 64. Whole sleep recordings were cut and concatenated to wakefulness, non-rapid eye movement stage 1, stage 2, and stage 3, where segments smaller than eight time points were eliminated.

Human Propofol Anesthesia

The human propofol anesthesia dataset has been previously published.[26,27] This study was approved by Ethics Committee of Huashan Hospital, Fudan University, Shanghai, China. All participants gave written informed consent. The study included 14 subjects (male/female: 6/8; age: 32 to 36 yr) who were selected for elective resection of pituitary microadenoma *via* a transsphenoidal approach (less than 10 mm in diameter without sella expansion by radiologic and plasma

endocrinic indicators). The blinding method was not used, and there was no missing subject. Participants were American Society of Anesthesiologists (Schaumburg, Illinois) Physical Status I or II grade with no history of craniotomy, cerebral neuropathy, or vital organs dysfunction.

By target-controlled infusion, we sustained 1.3 μg · kg^{-1} effect-site concentration for sedation state. To facilitate endotracheal intubation, remifentanil (1.0 μg · kg^{-1}) and succinylcholine (1.5 mg · kg^{-1}) was intravenously administrated. For general (deep) anesthesia state, we maintained the stable effect-site concentration (4.0 μg · kg^{-1}), which reliably kept patients in an unconscious state. Propofol effects on the brain are assumed to be not affected by other medications like analgesic remifentanil and depolarized neuromuscular relaxant succinylcholine because they are rapidly removed from plasma. During general anesthesia, intermittent positive pressure ventilation was used with tidal volume 8 to 10 ml · kg^{-1}, respiratory rate 10 to 12 beats per minute, and end-tidal pressure of carbon dioxide 35 to 40 mmHg. In the postoperative follow-up, no subject reported any memory of the anesthetic state during the functional magnetic resonance imaging scanning and surgical procedure.

A Siemens 3T scanner (Siemens MAGNETOM, Germany) was used to extract whole brain gradient echo-planar images (number of slices = 33, repetition-time/echo-time = 2,000/30 ms, slice thickness = 5 mm, field of view = 210 mm, flip angle = 90°, image matrix: 64 × 64). Three 8-min resting-state scans were recorded in wakefulness, sedation, and general anesthesia. High-resolution anatomical images were obtained. Before sedation scanning, subjects were given intravenously hydroxyethyl starch (500 ml) to prevent hypotension caused by propofol-induced vasodilation.

Rat Propofol Anesthesia

The experiment was performed on 12 adult male Sprague-Dawley rats in sequential order (age: 8 to 10 weeks; weight: 280 to 320 g; Shanghai Sippr-BK Laboratory Animal Co. Ltd., China). The blinding method was not used, and there were no missing data. The study protocol was approved by the Institutional Animal Care and Use Committee of Medical College, Fudan University. The experiment was carried out in compliance with the Guide for the Care and Use of Laboratory Animals, and Animal Research Reporting *In Vivo* Experiments guidelines. All animals were housed in a temperature-controlled facility with a reverse light-dark cycle (lights on at 6:00 AM) for at least 7 days before the experiment and had *ad libitum* access to food and water. We used only male animals for the following considerations: (1) female rats may introduce uncontrolled variables caused by hormonal fluctuations associated with the female reproductive cycle; (2) there may be potential sex differences in response to propofol dosages (same dosage but distinct behavioral responsiveness), which may pose technique challenges for animal experimental settings; (3) we followed the majority of functional magnetic resonance imaging studies in rats, where adult male rats were commonly used.

All the rats were first settled in a rat fixator in the prone position and received tail vein cannulation. Propofol anesthetic was induced with a 20 mg · kg^{-1} intravenous propofol bolus followed by 20 mg · kg^{-1} · h^{-1} propofol continuous intravenous infusion. They were then turned to the supine position for endotracheal intubation rapidly. After confirmation of the tube position, rats were given neuromuscular blocker rocuronium and ventilated by a volume-cycled magnetic resonance compatible rodent ventilator (SAR-1000, CWE, USA), with a mixture of oxygen/air (30/70), at 50 to 60 pushes per minute and 4.5 to 5.0 ml tidal volume delivered at a flow rate of 5 l/min. The rat's core temperature was maintained at 37 ± 0.5°C by a heated blanket. Rats continuously received infusion of 20 mg · kg^{-1} · h^{-1} propofol at least 30 min before first functional magnetic resonance imaging scan *via* 5-m infusion line connected to a Graseby TM 3500 target-controlled infusion Syringe Pump (Smiths Medical, United Kingdom). During the functional magnetic resonance imaging procedure, each rat was successively administrated propofol from 20 mg · kg^{-1} · h^{-1}, then 40 mg · kg^{-1} · h^{-1}, to 80 mg · kg^{-1} · h^{-1}, with a 30-min interval during which the propofol dosage was adjusted by changing the infusion rate on the pump.

To understand the physiologic changes at three different propofol dosages during mechanical ventilation, a separate group of three rats was examined outside the scanner, with the same protocol as in the functional magnetic resonance imaging procedure. Briefly, after tail vein cannulation and endotracheal intubation, sterile 2% lidocaine was administered subcutaneously for local anesthesia, and femoral artery cannulation was performed. Then we monitored arterial blood pressure and heart rate on the monitor (Datex Ohmeda S/5, Finland) and took an arterial blood sample at each propofol dosage to perform arterial blood gas analysis. The rats used for the functional magnetic resonance imaging study and physiologic measurements were executed with intravenous propofol and rocuronium for euthanasia after the experiment.

The functional magnetic resonance imaging data were acquired on a 7T Bruker Biospec system (Bruker BioSpin, Germany) in the supine position with a volume transmit/surface receive coil configuration. Three resting-state functional scans were taken with a single-shot echo-planar imaging sequence at low (20 mg · kg^{-1} · h^{-1}), medium (40 mg · kg^{-1} · h^{-1}), and high dosages (80 mg · kg^{-1} · h^{-1},) of propofol with the following parameters: number of slices = 80, repetition-time/echo-time = 4,000/16 ms, slice thickness = 0.3 mm, field of view = 35 mm × 35 mm, flip angle = 90°, image matrix = 96 × 96, repetition = 100. High-resolution anatomical images were obtained. We increased propofol dosage incrementally by changing the infusion rate at the end of each resting scan and waited 15 min for equilibrium at each propofol dosage, followed by the subsequent resting

state scans. The muscle relaxant rocuronium was given intravenously every 30 min to eliminate artifacts from spontaneous respiration and involuntary movement.

Patients with Disorders of Consciousness

The dataset of patients with disorders of consciousness has been previously published.[26,28,29] The dataset included 21 patients (male/female: 18/3) with disorders of consciousness (patients with disorders of consciousness) and 28 healthy control subjects (male/female: 14/14). The patients with disorders of consciousness were assessed using the Coma Recovery Scale-Revised[30] on the day of functional magnetic resonance imaging scanning. Thirteen patients were diagnosed as unresponsive wakefulness syndrome, and eight were diagnosed as minimally conscious state. There were no missing subjects in the analysis. For the healthy controls, none had a history of neurologic or psychiatric disorders, nor were they taking any kind of medication. Informed written consent was obtained from the patients' legal representatives, and from the healthy participants. The study was also approved by the Ethics Committee of Shanghai Huashan Hospital, Fudan University.

The functional magnetic resonance imaging data were acquired on Siemens 3T scanner. Echo-planar images covered the whole brain: number of slices = 33, repetition-time/echo-time = 2,000/35 ms, slice thickness = 4 mm, field of view = 256 mm, flip angle = 90°, image matrix = 64 × 64. Two hundred echo-planar imaging volumes as well as high-resolution anatomical images were acquired.

Data Preprocessing

Preprocessing steps were implemented in Analysis of Functional NeuroImages (https://afni.nimh.nih.gov/) including (1) discarding the first four frames of each functional magnetic resonance imaging run; (2) slice timing correction; (3) rigid body correction/realignment within and across runs; (4) coregistration with high-resolution anatomical images; (5) spatial normalization into Talaraich stereotactic space; (6) resampling to 3 × 3 × 3 mm^3 voxels; (7) regressing out linear and nonlinear drift, head motion and its temporal derivative, mean time series from the white matter and cerebrospinal fluid to control for physiologic and nonneural noise, and band-pass filtered to 0.01 to 0.10 Hz; (8) spatial smoothing with 6 mm full-width at half-maximum isotropic Gaussian kernel; (9) the time-course per voxel of each run was z-score normalized, accounting for differences in variance of nonneural origin (*e.g.,* distance from head coil)[31,32]; and (10) the issue of head motion artifacts was addressed rigorously based on previous studies.[33,34] Frame-wise displacement motion censoring was calculated using frame-wise Euclidean Norm (square root of the sum squares) of the six-dimension motion derivatives. A frame and its each previous frame were censored out from the original data if the given frame's displacement is above 0.4 mm (0.1 mm for rats).[26,35] Simultaneous cardiac and respiratory data (time locked to the functional magnetic resonance imaging signal acquisition) were not available due to the technical difficulties in the clinical settings. Nevertheless, the potential effects of physiologic noise were controlled by regressing out time courses based on non–gray matter signals and band-pass filtering during the above preprocessing steps. Since our study focuses on global signal, global signal regression will terminate any effects by global signal. Therefore, global signal regression was not done for the analysis. This was in line with the recommendations that it is reasonable to leave out global signal regression if the scientific question requires it.[5]

Global Signal Measurements

For each subject (or each state), we first extracted the average functional magnetic resonance imaging time series across all voxels in the gray matter, namely global signal. The SD of the global signal time series was defined as the global signal amplitude. We computed Pearson correlations between the global signal and the signal of each voxel in the gray matter. This yielded a whole-brain voxel-wise correlation map with a correlation coefficient (Fischer's Z transformed) per voxel. The gray matter average of correlation coefficients was defined as global signal functional connectivity.

The whole-brain voxel-wise correlation map derived during global signal functional connectivity calculation was defined as the global signal topography. Next, we adopted a well-established node template[36] that had been slightly modified for a previous study[26] containing 10 functional networks: subcortical, dorsal attention, ventral attention, default mode, frontoparietal task control, cingulo-opercular task control, salience, sensory/somatomotor, auditory, and visual networks. The averaged correlation coefficient (Fischer's Z transformed) across voxels for each network was extracted from the whole-brain correlation map, namely global-to-network functional connectivity, which indexes the degree to which the signal of each network is temporally coordinated with the global signal. This analysis was not done on the rat data as there is no agreeable brain network coordinate between rats and humans.

Statistical Analysis

The global signal amplitude, global signal functional connectivity, and global signal topography (network- and voxel-wise) were computed for each dataset; human natural sleep: wakefulness, non-rapid eye movement stage 1, stage 2, and stage 3; human propofol anesthesia: wakefulness, sedation, and general anesthesia; rat propofol anesthesia: low, medium, and high dose of propofol; and patients with disorders of consciousness: healthy control, minimally conscious state, and unresponsive wakefulness syndrome. Second-level analyses included the following: (1) Spearman rank correlation analyses between global signal amplitude (and global signal functional connectivity) and level of consciousness

(assigned as ranks) were performed across human and rat subjects, respectively, with a 95% CI based on 1,000 bootstrap samples. The wakefulness state in humans (or low dosage of propofol in rats) was ranked at 3; intermediate states (non-rapid eye movement stage 1 and stage 2 of sleep, sedation, and minimally conscious state in humans; medium dosage of propofol in rats) were ranked at 2; and unconscious states (non-rapid eye movement stage 3 of sleep, general anesthesia, and unresponsive wakefulness syndrome in humans; high dosage of propofol in rats) were ranked as 1. (2) To assay the main treatment effects of global signal amplitude (and global signal functional connectivity) on the level of consciousness, Friedman's tests were performed for paired samples (human natural sleep, human propofol anesthesia, and rat propofol anesthesia), and Kruskal–Wallis tests were performed for unpaired samples (patients with disorders of consciousness). (3) *Post hoc* tests were performed with Wilcoxon (paired samples) and Mann–Whitney (unpaired samples) tests on the global signal amplitude (and global signal functional connectivity). (4) To assay the state differences in the global signal topography at the network level, Wilcoxon and Mann–Whitney tests were performed for the contrasts of wakefulness *versus* unconsciousness states (non-rapid eye movement stage 3 of sleep, general anesthesia, and unresponsive wakefulness syndrome), as well as between different unconsciousness states. For 3 and 4, all tests were two-tailed. Using the Benjamini–Hochberg procedure, results in 3 were false discovery rate–corrected for multiple comparisons for each dataset (*e.g.,* for natural sleep there are four stages, so we correct for six comparisons) and thresholded at $\alpha = 0.05$. Results in 4 were false discovery rate–corrected for multiple comparisons across networks for each dataset (*e.g.,* 10 comparisons per dataset) and thresholded at $\alpha = 0.05$. (5) Whole-brain nonparametric tests for wakefulness *versus* unconsciousness states, as well as between different unconsciousness states, were performed for the global signal topography at the voxel level. The resulting delta-maps were thresholded at $\alpha = 0.05$ at the cluster level by Analysis of Functional NeuroImages function: 3dWilcoxon (paired samples) and 3dMannWhitney (unpaired samples).

Results

Global Signal Amplitude and Global Signal Functional Connectivity Decrease across States of Consciousness

We observed a gradual reduction in the global temporal coordination of brain activity when consciousness was reduced to a state in which subjects are still arousable or show residual behavioral signs of consciousness (non-rapid eye movement stage 1 and stage 2 of sleep, sedation, and minimally conscious state). We found a profound reduction of global temporal coordination during states in which subjects are generally considered to be unconscious (non-rapid eye movement stage 3 of sleep, general anesthesia, and unresponsive wakefulness syndrome) in humans and propofol anesthesia in rats (fig. 1). This was quantified by Spearman rank correlations between the global signal amplitude (and global signal functional connectivity) and the level of consciousness. We found statistically significant positive correlations in humans (rho = 0.41, $P < 0.001$, 95% CI, 0.27–0.53) and rats (rho = 0.53, $P < 0.001$, 95% CI, 0.20–0.78) for global signal amplitude, and in humans (rho = 0.41, $P < 0.001$, 95% CI, 0.27–0.53) and rats (rho = 0.55, $P < 0.001$, 95% CI, 0.24–0.80) for global signal functional connectivity.

Statistically significant treatment effects were present in global signal amplitude (human natural sleep: $P = 0.003$, chi-square = 14.20; human propofol anesthesia: $P = 0.005$, chi-square = 10.43; rat propofol anesthesia: $P = 0.028$, chi-square = 7.17; disorder of consciousness: $P < 0.001$, chi-square = 18.04), and global signal functional connectivity (human natural sleep: $P = 0.002$, chi-square = 14.73; human propofol anesthesia: $P = 0.005$, chi-square = 10.43; rat propofol anesthesia: $P = 0.017$, chi-square = 8.17; disorder of consciousness: $P < 0.001$, chi-square = 17.73; table 1). *Post hoc* analysis showed a statistically significant reduction of global signal amplitude and global signal functional connectivity in various unconscious states. For global signal amplitude (fig. 2A), the comparisons were wakefulness (median [1st, 3rd quartile], 0.46 [0.21, 0.50]) *versus* non-rapid eye movement stage 3 of sleep (0.30 [0.24, 0.32]; $P = 0.035$), wakefulness (0.36 [0.31, 0.42]) *versus* general anesthesia (0.25 [0.21, 0.28]; $P < 0.001$), healthy controls (0.30 [0.27, 0.37]) *versus* unresponsive wakefulness syndrome (0.22 [0.15, 0.24]; $P < 0.001$), and low dose (0.07 [0.06, 0.08] *versus* high dose of propofol (0.04 [0.03, 0.05]; $P = 0.028$) in rats. For global signal functional connectivity (fig. 2B), the comparisons were wakefulness (0.51 [0.22, 0.59]) *versus* non-rapid eye movement stage 3 of sleep (0.31 [0.25, 0.33]; $P = 0.035$), wakefulness (0.40 [0.32, 0.51]) *versus* general anesthesia (0.26 [0.22, 0.29]; $P = 0.001$), healthy controls (0.32 [0.28, 0.39]) *versus* unresponsive wakefulness syndrome (0.23 [0.15, 0.26]; $P < 0.001$), and low dose (0.15 [0.13, 0.18]) *versus* high dose of propofol (0.07 [0.06, 0.11]; $P = 0.015$) in rats.

Global signal amplitude and global signal functional connectivity yielded similar results, which was expected given that the two measurements are mathematically related with both quantifying the shared variances across voxels.[11,37] In fact, statistically significant correlations (across subjects) between global signal amplitude and global signal functional connectivity were observed in both humans (rho = 0.99, $P < 0.001$, 95% CI, 0.98–0.99) and rats (rho = 0.97, $P < 0.001$, 95% CI, 0.93–0.99; fig. 2C). Collectively, the above results suggest a strong association between the net strength of overall brain connectivity (*i.e.*, global temporal coordination) and the level of consciousness.

In addition, we found no statistically significant sex effect (female *vs.* male; median [1st, 3rd quartile]) for either conscious or unconscious states in the human datasets. For global signal amplitude, the results were (0.39 [0.27, 0.49])

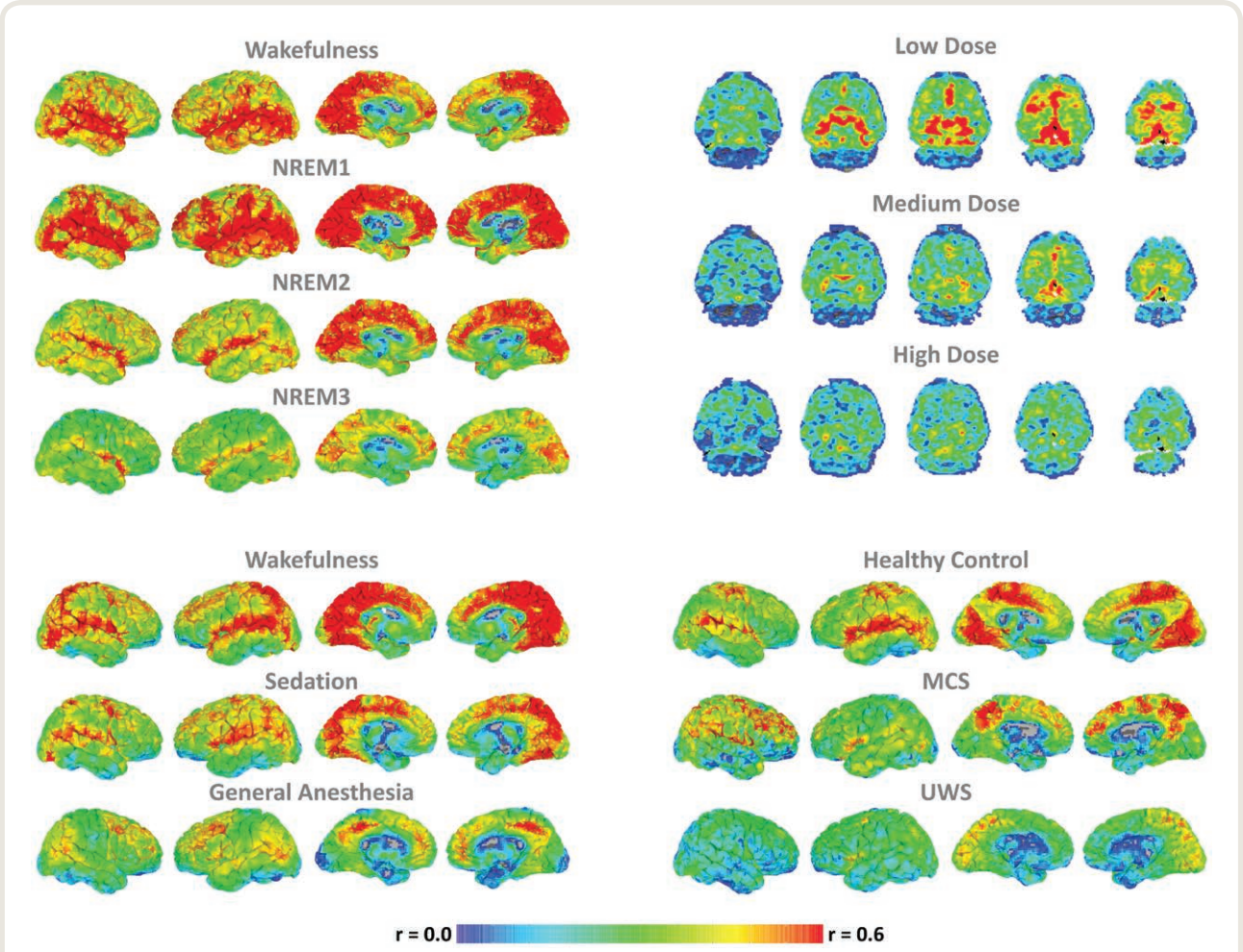

Fig. 1. Average whole-brain global signal correlation maps at the group level. (*Top left*) Human subjects in wakefulness, non-rapid eye movement stage 1 (NREM1), non-rapid eye movement stage 2 (NREM2), and non-rapid eye movement stage 3 (NREM3). (*Bottom left*) Human subjects receiving propofol infusion. (*Top right*) Rats receiving different doses of propofol. (*Bottom right*) Human subjects of healthy controls, patients with minimally conscious state (MCS), and unresponsive wakefulness syndrome (UWS). Of note, the distinctions in the images of the healthy controls during wakefulness may be due to the fact that different scanners or data acquisition parameters can affect the absolute value of the measurement.

versus (0.47 [0.22, 0.52]; $P = 0.730$) and (0.28 [0.23, 0.31]) *versus* (0.31 [0.24, 0.33]; $P = 0.730$) during wakefulness and non-rapid eye movement stage 3 of human sleep dataset, respectively, (0.38 [0.31, 0.44]) *versus* (0.36 [0.33, 0.37]; $P = 0.852$) and (0.26 [0.21, 0.28]) *versus* (0.25 [0.23, 0.28]; $P = 0.852$) during wakefulness and general anesthesia of human propofol dataset, respectively, and (0.30 [0.27, 0.35]) *versus* (0.31 [0.28, 0.44]; $P = 0.175$) in the healthy control group of neuropathologic patients (biologic sex analysis was not performed in patients due to the limited number of females). For global signal functional connectivity, the results were (0.42 [0.28, 0.56]) *versus* (0.52 [0.23, 0.59]; $P = 0.905$) and (0.29 [0.24, 0.32]) *versus* (0.33 [0.25, 0.35]; $P = 0.905$) during wakefulness and non-rapid eye movement stage 3 of human sleep dataset, respectively, (0.41 [0.32, 0.55]) *versus* (0.39 [0.34, 0.40]; $P = 0.852$) and (0.27 [0.21, 0.29]) *versus* (0.26 [0.24, 0.29]; $P = 0.852$) during wakefulness and general anesthesia of human propofol dataset, respectively, and (0.32 [0.28, 0.39]) *versus* (0.33 [0.29, 0.49]; $P = 0.175$) in the healthy control group of neuropathologic patients.

Global Signal Topography

We compared the global-to-network functional connectivity, indexing the degree to which the signal of each network is temporally coordinated with the global signal, between wakeful and unconscious states (non-rapid eye movement stage 3 of sleep, general anesthesia, and unresponsive wakefulness syndrome). Adopting a predefined network template (fig. 3A), we found statistical significance in reduced global-to-network functional connectivity in auditory,

Table 1. Statistics for Friedman Rest and Kruskal–Wallis Rest, *Post Hoc* Tests on Global Signal Amplitude, and Global Signal Functional Connectivity

	Global Signal Amplitude			Global Signal Functional Connectivity		
	Median [1st Quartile to 3rd Quartile]	Group Test	Wilcoxon Test	Median [1st Quartile to 3rd Quartile]	Group Test	Wilcoxon Test
Human natural sleep						
Wakefulness	0.46 [0.21 to 0.50]			0.51 [0.22 to 0.59]		
NREM1	0.43 [0.22 to 0.53]			0.49 [0.23 to 0.64]		
NREM2	0.42 [0.21 to 0.42]			0.46 [0.22 to 0.47]		
NREM3	0.30 [0.24 to 0.32]			0.31 [0.25 to 0.33]		
Friedman, *P*		0.003			0.002	
Friedman chi-square		14.20			14.73	
Wakefulness *vs.* NREM1, *P*			0.426			0.203
Wakefulness *vs.* NREM2, *P*			0.066			0.066
Wakefulness *vs.* NREM3, *P*			0.035			0.035
NREM1 *vs.* NREM2, *P*			0.066			0.066
NREM1 *vs.* NREM3, *P*			0.035			0.035
NREM2 *vs.* NREM3, *P*			0.066			0.066
Human propofol anesthesia						
Wakefulness	0.36 [0.31 to 0.42]			0.40 [0.32 to 0.51]		
Sedation	0.30 [0.22 to 0.37]			0.32 [0.23 to 0.41]		
Anesthesia	0.25 [0.21 to 0.28]			0.26 [0.22 to 0.29]		
Friedman, *P*		0.005			0.005	
Friedman chi-square		10.43			10.43	
Wakefulness *vs.* sedation, *P*			0.063			0.044
Wakefulness *vs.* anesthesia, *P*			0.001			0.001
Sedation *vs.* anesthesia, *P*			0.153			0.194
Rat propofol anesthesia						
Wakefulness	0.07 [0.06 to 0.08]			0.15 [0.13 to 0.18]		
Sedation	0.05 [0.05 to 0.05]			0.11 [0.09 to 0.12]		
Anesthesia	0.04 [0.03 to 0.05]			0.07 [0.06 to 0.11]		
Friedman, *P*		0.028			0.017	
Friedman chi-square		7.17			8.17	
Wakefulness *vs.* sedation, *P*			0.031			0.018
Wakefulness *vs.* anesthesia, *P*			0.028			0.015
Sedation *vs.* anesthesia, *P*			0.151			0.129
Disorder of consciousness						
Healthy control	0.30 [0.27 to 0.37]			0.32 [0.28 to 0.39]		
MCS	0.26 [0.19 to 0.29]			0.28 [0.19 to 0.32]		
UWS	0.22 [0.15 to 0.24]			0.23 [0.15 to 0.26]		
Kruskal–Wallis, *P*		< 0.001			< 0.001	
Kruskal–Wallis chi-square		18.04			17.73	
Healthy control *vs.* MCS, *P*			0.089			0.106
Healthy Control *vs.* UWS, *P*			< 0.001			< 0.001
MCS *vs.* UWS, *P*			0.158			0.138

Post hoc tests were performed with Wilcoxon test for Friedman test and Mann–Whitney test for Kruskal–Wallis test. All *post hoc P* values are false discovery rate–corrected ($\alpha = 0.05$) across the combinations of states (*i.e.,* for human natural sleep we correct for six comparisons). MCS, minimally conscious state; NREM1, non-rapid eye movement stage 1 of sleep; NREM2, non-rapid eye movement stage 2 of sleep; NREM3, non-rapid eye movement stage 3 of sleep; UWS, unresponsive wakefulness syndrome.

visual, sensory/somatomotor, ventral, and dorsal attention networks during non-rapid eye movement stage 3 of sleep (fig. 3B), and reduced global-to-network functional connectivity in all except cingulo-opercular, salience, and frontoparietal task control networks during general anesthesia (fig. 3C). Statistical significance in reduced global-to-network functional connectivity was observed in all networks in unresponsive wakefulness syndrome patients (fig. 3D). Statistics are reported in table 2. These results suggest that the reduction of global temporal coordination of brain activity (measured by global signal amplitude and global signal functional connectivity) during non-rapid eye movement stage 3 of sleep was likely due to selective decoupling of sensory and attention networks from the global activity. In contrast, during what is presumably complete loss of consciousness (general anesthesia and unresponsive wakefulness syndrome), the majority of functionally segregated networks were uncoupled from the global brain network. In addition, comparisons between different states of unconsciousness were performed at the network level. No statistically

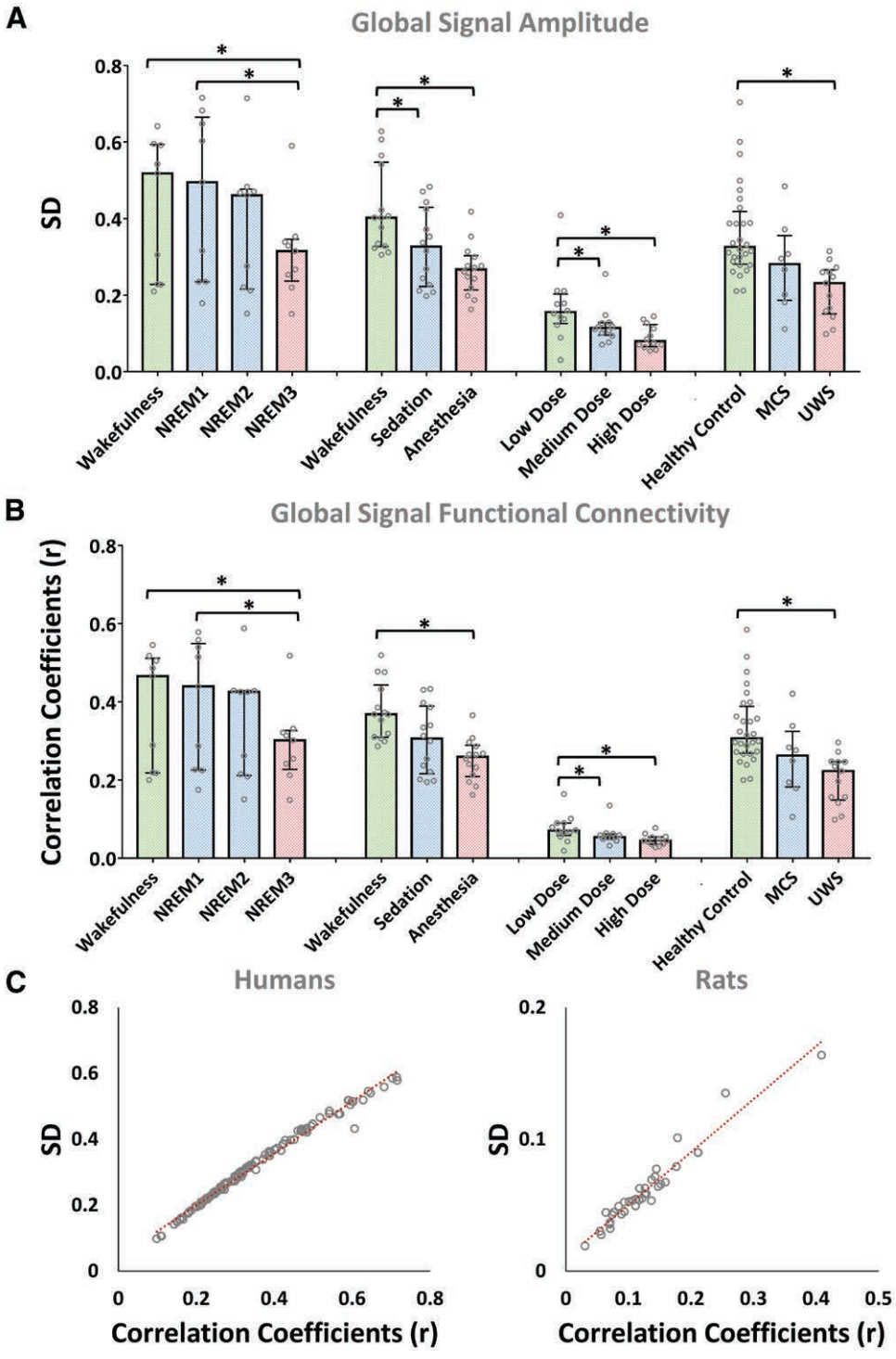

Fig. 2. Global signal amplitude and global signal functional connectivity. (*A*) Global signal amplitude as measured by the SD of the global signal time series. (*B*) Global signal functional connectivity as measured by the average correlation coefficient between the global signal and the signal of each voxel in gray matter. Human natural sleep dataset (n = 9) includes wakefulness, non-rapid eye movement stage 1 (NREM1), stage 2 (NREM2), and stage 3 (NREM3). Human propofol anesthesia dataset (n = 14) includes wakefulness, sedation, and general anesthesia. Rat propofol anesthesia dataset (male, n = 12) includes low, medium, and high dose. Dataset of disorders of consciousness includes healthy controls (n = 28), patients with minimally conscious state (MCS; n = 8), and unresponsive wakefulness syndrome (UWS; n = 13). *Significance at $\alpha = 0.05$ (corrected). *Bar graph* shows 1st quartile, median, and 3rd quartile. (*C*) Correlation between global signal amplitude and global signal functional connectivity across all human subjects and rats.

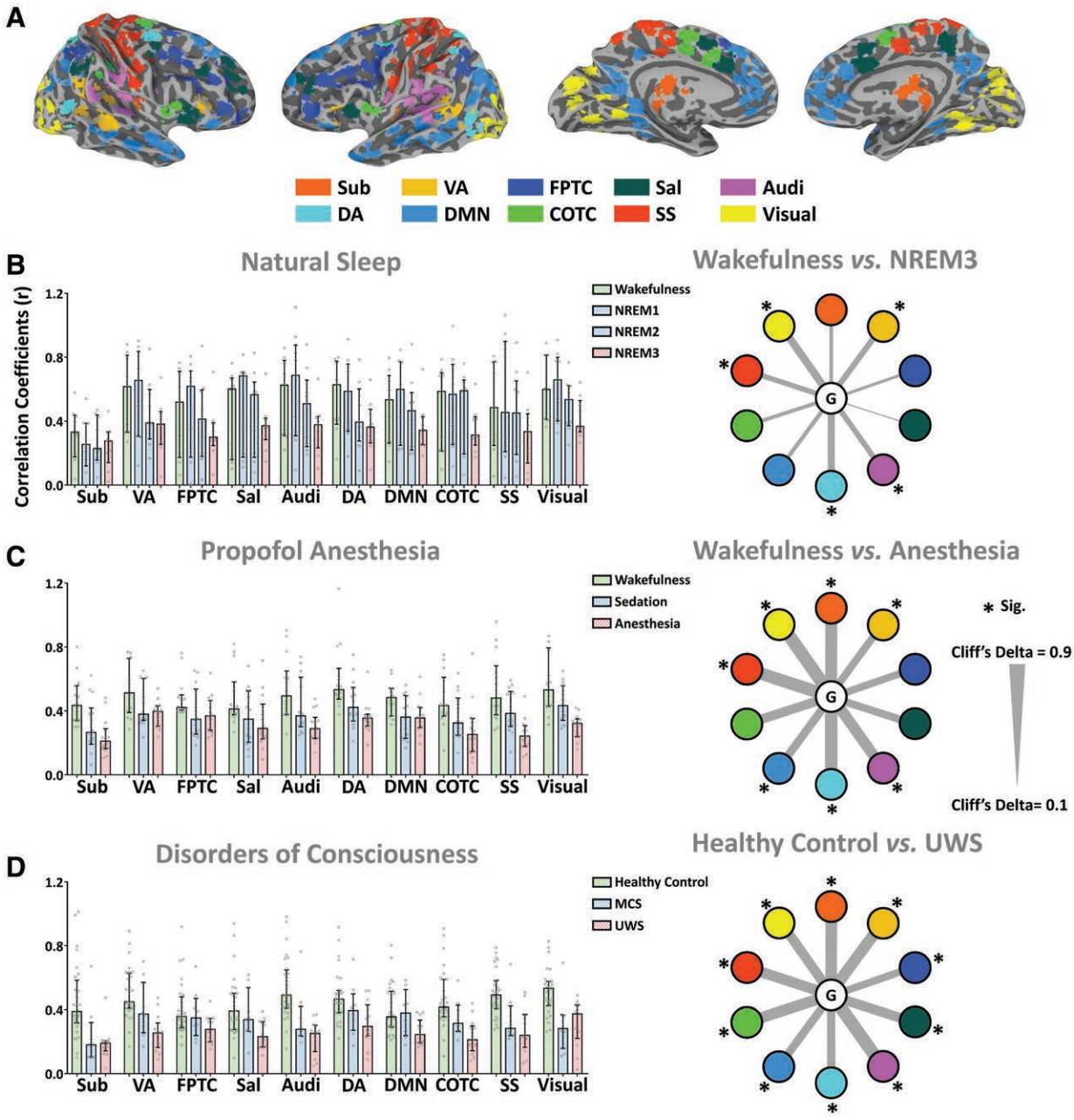

Fig. 3. Global signal topography at the network level. (*A*) Illustration of the predefined network template: subcortical (Sub), ventral attention (VA), frontoparietal task control (FPTC), salience (Sal), auditory (Audi), dorsal attention (DA), default mode (DMN), cingulo-opercular task control (COTC), sensory/somatomotor (SS), and visual (Visual). (*B–D*) Global-to-network functional connectivity in various human datasets. *Significance after false discovery rate correction ($\alpha = 0.05$). *Bar graph* shows 1st quartile, median and 3rd quartile. MCS, minimally conscious state; NREM1, non-rapid eye movement stage 1 of sleep; NREM2, non-rapid eye movement stage 2 of sleep; NREM3, non-rapid eye movement stage 3 of sleep; UWS, unresponsive wakefulness syndrome.

significant result was seen after multiple comparison corrections (uncorrected *P* values are reported in table 2).

The voxel-level topographical representation of the global signal showed relatively sparse changes, limited to sensory and attention networks, during non-rapid eye movement stage 3 of sleep, whereas it showed widespread changes during general anesthesia and in unresponsive wakefulness syndrome patients (fig. 4). Interestingly, there seemed to be distinct topographical changes in general anesthesia and in unresponsive wakefulness syndrome. Specifically, the peak clusters of

Table 2. Statistics for Global-to-network Functional Connectivity

	Sub	VA	FPTC	Sal	Audi	DA	DMN	COTC	SS	Visual
Comparison within conditions										
Human natural sleep, wakefulness *vs.* NREM3										
Wakefulness median	0.33	0.62	0.52	0.60	0.62	0.63	0.53	0.59	0.49	0.60
Wakefulness 1st quartile	0.19	0.33	0.19	0.17	0.31	0.40	0.27	0.22	0.26	0.41
Wakefulness 3rd quartile	0.43	0.80	0.70	0.66	0.77	0.77	0.67	0.70	0.77	0.81
NREM3 median	0.28	0.38	0.30	0.37	0.38	0.36	0.34	0.31	0.33	0.37
NREM3 1st quartile	0.17	0.26	0.26	0.32	0.26	0.27	0.25	0.27	0.17	0.35
NREM3 3rd quartile	0.33	0.45	0.38	0.41	0.43	0.46	0.42	0.42	0.43	0.51
Cliff's delta	0.23	0.41	0.21	0.09	0.38	0.48	0.28	0.26	0.36	0.53
P value	0.254	0.039	0.234	0.426	0.029	0.029	0.163	0.278	0.029	0.029
Human propofol anesthesia, wakefulness *vs.* anesthesia										
Wakefulness median	0.43	0.51	0.42	0.41	0.49	0.53	0.48	0.43	0.48	0.53
Wakefulness 1st quartile	0.34	0.40	0.41	0.38	0.38	0.48	0.37	0.37	0.38	0.43
Wakefulness 3rd quartile	0.56	0.73	0.49	0.53	0.61	0.62	0.54	0.59	0.64	0.78
Anesthesia median	0.21	0.40	0.37	0.29	0.29	0.36	0.36	0.25	0.24	0.32
Anesthesia 1st quartile	0.17	0.31	0.28	0.23	0.23	0.31	0.30	0.15	0.18	0.24
Anesthesia 3rd quartile	0.28	0.43	0.46	0.42	0.34	0.37	0.42	0.35	0.31	0.35
Cliff's delta	0.82	0.52	0.51	0.53	0.77	0.87	0.57	0.64	0.87	0.89
P value	0.004	0.015	0.068	0.055	0.006	0.002	0.014	0.052	0.002	0.001
Disorder of consciousness, healthy control *vs.* UWS										
Healthy control median	0.39	0.45	0.36	0.39	0.49	0.47	0.36	0.42	0.49	0.53
Healthy control 1st quartile	0.32	0.41	0.29	0.28	0.41	0.38	0.29	0.36	0.41	0.43
Healthy control 3rd quartile	0.56	0.62	0.47	0.50	0.64	0.52	0.51	0.59	0.58	0.58
UWS median	0.19	0.26	0.28	0.23	0.25	0.30	0.24	0.21	0.24	0.37
UWS 1st quartile	0.15	0.18	0.20	0.17	0.16	0.24	0.19	0.15	0.18	0.24
UWS 3rd quartile	0.20	0.30	0.34	0.32	0.30	0.42	0.32	0.29	0.37	0.43
Cliff's delta	0.79	0.79	0.52	0.68	0.89	0.57	0.57	0.77	0.73	0.68
P value	< 0.001	< 0.001	0.009	0.001	< 0.001	0.005	0.005	< 0.001	< 0.001	0.001
Comparison across conditions										
Human natural sleep (NREM3*)										
NREM3* median	–0.05	–0.19	–0.15	–0.07	–0.17	–0.19	–0.15	–0.16	–0.15	–0.23
NREM3* 1st quartile	–0.15	–0.31	–0.19	–0.13	–0.29	–0.28	–0.24	–0.21	–0.32	–0.25
NREM3* 3rd quartile	0.01	–0.12	–0.07	–0.03	–0.12	–0.09	–0.07	–0.06	–0.05	–0.08
Human propofol anesthesia (anesthesia*)										
Anesthesia* median	–0.25	–0.13	–0.11	–0.19	–0.25	–0.24	–0.12	–0.21	–0.30	–0.29
Anesthesia* 1st quartile	–0.29	–0.22	–0.20	–0.25	–0.31	–0.29	–0.18	–0.32	–0.36	–0.37
Anesthesia* 3rd quartile	–0.19	–0.10	–0.02	–0.05	–0.20	–0.23	–0.05	–0.12	–0.23	–0.26
Disorder of consciousness (UWS*)										
UWS* median	–0.26	–0.25	–0.13	–0.20	–0.28	–0.19	–0.16	–0.26	–0.26	–0.14
UWS* 1st quartile	–0.30	–0.33	–0.20	–0.26	–0.37	–0.25	–0.21	–0.31	–0.33	–0.27
UWS* 3rd quartile	–0.25	–0.21	–0.06	–0.10	–0.23	–0.07	–0.09	–0.18	–0.13	–0.09
Human natural sleep (NREM3*) *vs.* human propofol anesthesia (anesthesia*)										
Cliff's delta	0.56	–0.24	–0.10	0.32	0.17	0.22	–0.13	0.33	0.35	0.67
P value (uncorr.)	0.030	0.361	0.729	0.219	0.508	0.395	0.637	0.197	0.176	0.009
Human natural sleep (NREM3*) *vs.* disorder of consciousness (UWS*)										
Cliff's delta	0.69	0.21	–0.03	0.56	0.52	–0.08	–0.04	0.50	0.16	0.03
P value (uncorr.)	0.008	0.423	0.947	0.033	0.045	0.789	0.894	0.053	0.548	0.947
Human propofol anesthesia (anesthesia*) *vs.* disorder of consciousness (UWS*)										
Cliff's delta	0.18	0.55	0.08	0.09	0.30	–0.36	0.18	0.15	–0.23	–0.53
P value (uncorr.)	0.452	0.016	0.752	0.716	0.198	0.115	0.452	0.512	0.320	0.021

Only *P* values for "Comparison within conditions" have been false discovery rate–corrected ($\alpha = 0.05$). *Normalized by subtracting mean of base state (Wakefulness, Healthy control). Audi, auditory; COTC, cingulo-opercular task control; DA, dorsal attention; DMN, default mode; FPTC, frontoparietal task control; MCS, minimally conscious state; NREM3, non-rapid eye movement stage 3 of sleep; Sal, salience; SS, sensory/somatomotor; Sub, subcortical; UWS, unresponsive wakefulness syndrome; VA, ventral attention.

group differences were located in the precuneus in general anesthesia, and in the anterior cingulate cortex in unresponsive wakefulness syndrome. Moreover, statistically significant regional differences between unconscious conditions were found in the thalamus (non-rapid eye movement stage 3 > unresponsive wakefulness syndrome > general anesthesia), precuneus (non-rapid eye movement stage 3 = unresponsive wakefulness syndrome > general anesthesia), and anterior cingulate cortex (non-rapid eye movement stage 3 = general anesthesia > unresponsive wakefulness syndrome).

Discussion

The goal of this investigation was to examine how the functional magnetic resonance imaging–based global brain signal

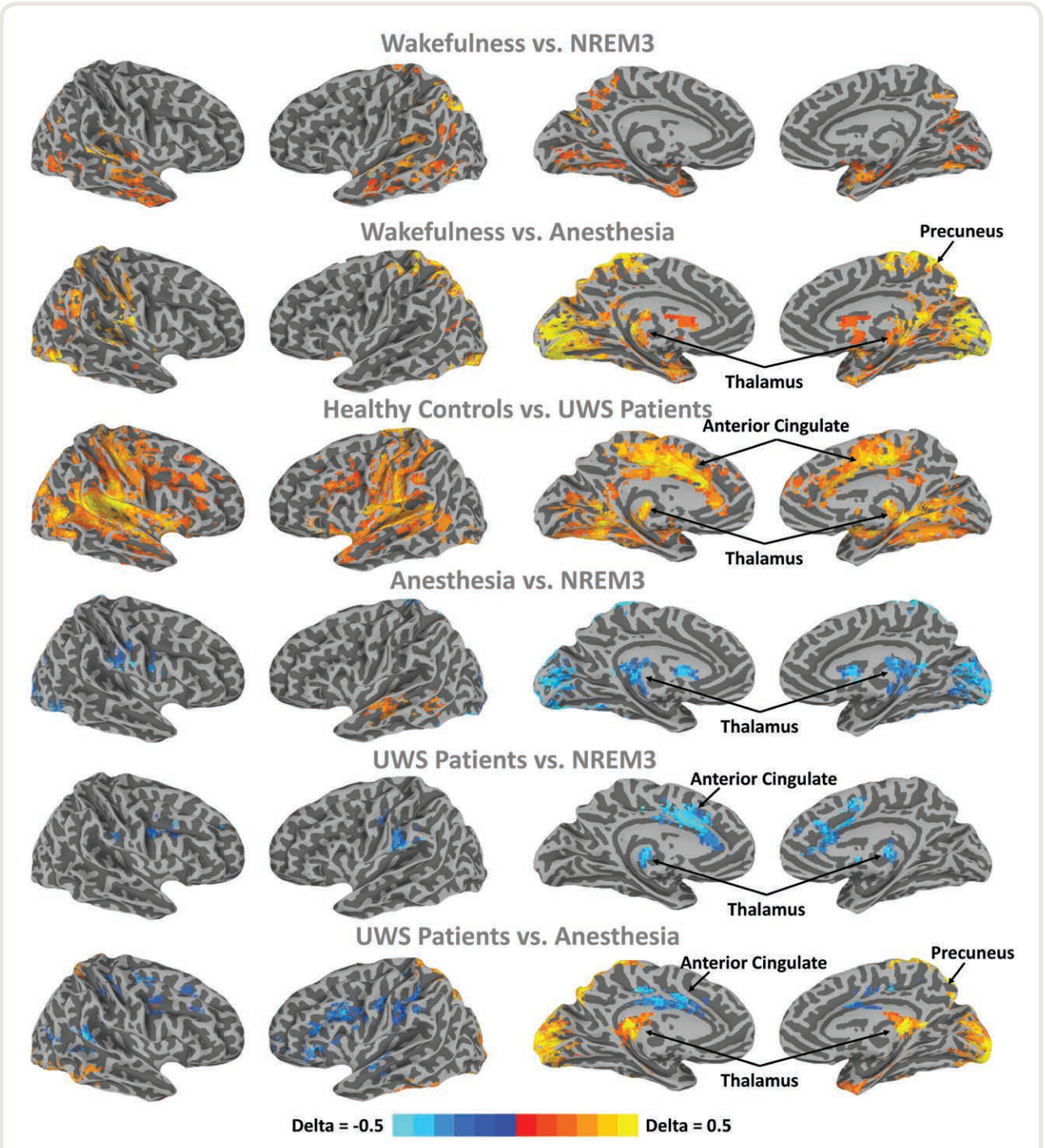

Fig. 4. Global signal topography at the voxel level. Delta-maps (Cliff's delta or *d*) from whole-brain voxel-wise nonparametric tests. (*Top three rows*) Comparison within conditions. (*Bottom three rows*) Comparison across conditions. Delta-maps were thresholded at $\alpha = 0.05$ at the cluster level. The locations for the peak cluster of within condition differences (precuneus and anterior cingulate) are marked. NREM3, non-rapid eye movement stage 3 of sleep; UWS, unresponsive wakefulness syndrome.

changes across the spectrum of different states of consciousness. We demonstrated a strong association between the net strength of overall brain connectivity (measured by global signal amplitude and global signal functional connectivity) and the level of consciousness in both humans and rats. Furthermore, we found specific alterations in the global signal topography during unconsciousness states. Non-rapid eye movement stage 3 of sleep was characterized by a decoupling

of sensory and attention networks from the global network. General anesthesia and unresponsive wakefulness syndrome were characterized by a dissociation of the majority of functionally segregated networks from the global network. Finally, the reduction of global temporal coordination of brain activity during general anesthesia and in unresponsive wakefulness syndrome patients seems to be mediated by distinct neuroanatomic foci (*e.g.,* precuneus and anterior cingulate cortices). Collectively, our findings suggest that the global temporal coordination defines the coarse-grained state of consciousness *versus* unconsciousness, while the relationship of the global and local signals defines the particular qualities of that unconscious state, which may be determinants of reversibility.

Our findings are in agreement with neuroimaging studies suggesting that global functional connectivity of the brain is an indicator of level of consciousness in both humans[26,29,38–40] and rodents.[41,42] The current study adds support to this proposition based on the assessment of the global brain signal for the first time. Furthermore, our findings on the net strength of overall brain connectivity offer a complementary view with regard to the alterations of functional network interactions during loss of consciousness.[43]

Importantly, we identified both state-invariant and state-specific features of the global signal during various states of consciousness. There was a clear correlation of global signal amplitude and global signal functional connectivity with level of consciousness that was, in terms of unconsciousness, independent of the physiologic, pharmacologic, or pathologic etiology. However, the relationship of the global signal to local signals demonstrated specificity, as we would expect from these distinct states.

Global brain activity makes up a large portion of the resting-state functional magnetic resonance imaging signal and appears related to fluctuations in arousal and vigilance,[8,9,16] memory consolidation,[44] and psychiatric symptoms.[7] Recent studies have provided evidence for a link between functional magnetic resonance imaging–derived global signal and electrophysiology.[8,16,19] Nevertheless, the exact origin and mechanism of the global brain signal and its functional role remain unsettled. The global signal could result from either a common source (*e.g.,* thalamus or basal forebrain) that broadcasts local signals to the rest of the brain[8,16] or from a widespread interaction of functional networks *via* feedback pathways.[37] Our results on the topographical representation of global signal map suggest multiple sources of the global signal. Although a reduction of global signal accompanies loss of consciousness due to various reasons, some of the networks and focal brain regions (*e.g.,* precuneus and anterior cingulate) that are involved in this phenomenon may be different. This may be due to the fact that different conditions (*e.g.,* natural sleep, anesthesia, neuropathologic disorders) involve different molecular mechanisms, neural circuits, and brain functions, which likely result in different global signal topographies.

Although our results may imply that unconsciousness results in loss of coordination in neuronal activity, caveats need to be pointed out when generalizing functional magnetic resonance imaging findings to electroencephalographic findings (and *vice versa*). Many electroencephalographic studies have documented that unconsciousness is associated with an increase in neuronal activity correlations, presumably reflecting correlated depolarization of cortical neurons.[45,46] For instance, low-frequency high-amplitude electroencephalographic oscillations (*e.g.,* slow-wave activity) are a neural signature for non-rapid eye movement stage 3 of sleep and anesthetic-induced unconsciousness.[47] Notably, electroencephalographic recordings and functional magnetic resonance imaging–derived blood oxygen level–dependent time courses are inherently different signals, measuring different types of brain activity.[48] To understand the apparent counterpoint between functional magnetic resonance imaging and electroencephalographic studies, one may revisit the possible relationship between electrophysiologic and blood oxygen level–dependent signals. As reported by Schölvinck *et al.*,[19] the power of local field potentials at different frequencies (below 12 Hz and above 40 Hz) were both correlated with global blood oxygen level–dependent signal, whereas the power between 12 and 40 Hz was not found to have a significant relationship to global blood oxygen level–dependent signal. As different states of sleep and unconscious states are characterized by differences in electrophysiologic power spectra relative to conscious wakefulness,[47] it is possible that neuronal activity is coordinated in the state of unconsciousness but in a frequency band that is not reflected in the global fluctuations of blood oxygen level–dependent signals. Furthermore, as shown in the same study,[19] the degree of correlation between global blood oxygen level–dependent signals and local field potentials is state-dependent. Specifically, when the level of arousal wanes, so does the correlation between global blood oxygen level–dependent signals and local field potentials. Therefore, in the case of a conscious brain, the global blood oxygen level–dependent signal does offer some, albeit limited, information about brain activity, but in the case of diminished consciousness, this information may be lost. Taken together, loss of global fluctuations in blood oxygen level–dependent signal during unconsciousness does not necessarily imply lack of coordination of neuronal activity in general. Future studies with concurrent functional magnetic resonance imaging and electrophysiology may help disentangle those conditions, and hopefully provide deeper insight into the global brain activity in relation to the level of consciousness.

A few limitations of our study are recognized. First, although this study covered a variety of unconscious conditions, it remains unable to clearly distinguish between behavioral arousal and conscious awareness. Nevertheless, given that in unresponsive wakefulness syndrome patients, arousal is relatively preserved while awareness is suppressed, the reduction of global temporal coordination of brain activity would likely reflect the level of awareness more than that of arousal. Second, our study focused on the level

of consciousness while neglecting other dimensions, such as phenomenal experience or conscious access.[49] We cannot address, for example, how the changes in global signal affect the processing of specific contents. Third, we did not find a statistically significant sex effect in the human groups. However, due to the limited sample size in human subjects and the fact that only male animals were studied, we were not able to exclude possible sex effects in terms of global brain signal alteration during unconsciousness. This possibility will be examined in future studies. Last, we did not perform *a priori* statistical power calculation before acquiring our data. However, we applied a pooled data analysis and drew the major conclusion, *i.e.,* a breakdown of global temporal coordination during unconsciousness, based on the results across physiologic, pharmacologic, and pathologic states of unconsciousness (n = 36 in humans; n = 12 in rats). We believe that the consistency of results found across different types of unconsciousness enhances the reliability of the observed effects. The specific patterns of decoupling between local regions and global activity in different kinds of unconscious states were based on unpooled analysis with limited sample size, which may be considered as exploratory results that warrant future studies with a larger sample size.

Conclusions

The breakdown of global temporal coordination across the brain seems to be a general, species-invariant finding across physiologic, pharmacologic, and pathologic states of unconsciousness. However, variations in signal topography show state-specific patterns that might differentiate sleep, anesthesia, and disorders of consciousness.

Research Support

This research was supported by Medical Guidance Supporting Project from Shanghai Municipal Science and Technology Commission (Shanghai, China; No. 17411961400) to Dr. Zhang; the Canada Institute of Health Research to Dr. Doyon; the Michael Smith Foundation from the Canada Institute of Health Research, National Natural Science Foundation of China (China, No. 31271195), and European Union's Horizon 2020 Framework Programme for Research and Innovation under the Specific Grant Agreement No. 785907 (Human Brain Project Specific Grant Agreement 2, European Union) to Dr. Northoff; and grants from the National Institute of General Medical Sciences of the National Institutes of Health (Bethesda, Maryland; R01-GM103894) to Dr. Hudetz. The content is solely the responsibility of the authors and does not necessarily represent the official views of the National Institutes of Health.

Competing Interests

The authors declare no competing interests.

Correspondence

Address correspondence to Dr. Zhang: Department of Anesthesiology, Huashan Hospital, Fudan University, #12, Wulumuqi Middle Road, Shanghai, 200040, China. snapzhang@aliyun.com. Information on purchasing reprints may be found at www.anesthesiology.org or on the masthead page at the beginning of this issue. Anesthesiology's articles are made freely accessible to all readers, for personal use only, 6 months from the cover date of the issue.

References

1. Tononi G, Boly M, Massimini M, Koch C: Integrated information theory: From consciousness to its physical substrate. Nat Rev Neurosci 2016; 17:450–61
2. Dehaene S, Charles L, King JR, Marti S: Toward a computational theory of conscious processing. Curr Opin Neurobiol 2014; 25:76–84
3. Dehaene S, Changeux JP: Experimental and theoretical approaches to conscious processing. Neuron 2011; 70:200–27
4. Northoff G, Huang Z: How do the brain's time and space mediate consciousness and its different dimensions? Temporo-spatial theory of consciousness (TTC). Neurosci Biobehav Rev 2017; 80:630–45
5. Murphy K, Fox MD: Towards a consensus regarding global signal regression for resting state functional connectivity MRI. Neuroimage 2017; 154:169–73
6. Yang GJ, Murray JD, Repovs G, Cole MW, Savic A, Glasser MF, Pittenger C, Krystal JH, Wang XJ, Pearlson GD, Glahn DC, Anticevic A: Altered global brain signal in schizophrenia. Proc Natl Acad Sci USA 2014; 111:7438–43
7. Yang GJ, Murray JD, Glasser M, Pearlson GD, Krystal JH, Schleifer C, Repovs G, Anticevic A: Altered global signal topography in schizophrenia. Cereb Cortex 2017; 27:5156–69
8. Liu X, de Zwart JA, Schölvinck ML, Chang C, Ye FQ, Leopold DA, Duyn JH: Subcortical evidence for a contribution of arousal to fMRI studies of brain activity. Nat Commun 2018; 9:395
9. Chang C, Leopold DA, Schölvinck ML, Mandelkow H, Picchioni D, Liu X, Ye FQ, Turchi JN, Duyn JH: Tracking brain arousal fluctuations with fMRI. Proc Natl Acad Sci USA 2016; 113:4518–23
10. Nalci A, Rao BD, Liu TT: Global signal regression acts as a temporal downweighting process in resting-state fMRI. Neuroimage 2017; 152:602–18
11. Liu TT, Nalci A, Falahpour M: The global signal in fMRI: Nuisance or information? Neuroimage 2017; 150:213–29
12. Zhang J, Magioncalda P, Huang Z, Tan Z, Hu X, Hu Z, Conio B, Amore M, Inglese M, Martino M, Northoff G: Altered global signal topography and its different regional

localization in motor cortex and hippocampus in mania and depression. Schizophr Bull 2019; 45:902–10
13. Power JD, Laumann TO, Plitt M, Martin A, Petersen SE: On global fMRI signals and simulations. Trends Cogn Sci 2017; 21:911–3
14. Wen H, Liu Z: Broadband electrophysiological dynamics contribute to global resting-state fMRI signal. J Neurosci 2016; 36:6030–40
15. Billings J, Keilholz S: The not-so-global blood oxygen level-dependent signal. Brain Connect 2018; 8:121–8
16. Turchi J, Chang C, Ye FQ, Russ BE, Yu DK, Cortes CR, Monosov IE, Duyn JH, Leopold DA: The basal forebrain regulates global resting-state fMRI fluctuations. Neuron 2018; 97:940–952.e4
17. Liu TT: Reprint of 'Noise contributions to the fMRI signal: An overview'. Neuroimage 2017; 154:4–14
18. Shulman RG, Hyder F, Rothman DL: Baseline brain energy supports the state of consciousness. Proc Natl Acad Sci USA 2009; 106:11096–101
19. Schölvinck ML, Maier A, Ye FQ, Duyn JH, Leopold DA: Neural basis of global resting-state fMRI activity. Proc Natl Acad Sci USA 2010; 107:10238–43
20. Hahamy A, Calhoun V, Pearlson G, Harel M, Stern N, Attar F, Malach R, Salomon R: Save the global: Global signal connectivity as a tool for studying clinical populations with functional magnetic resonance imaging. Brain Connect 2014; 4:395–403
21. Ponce-Alvarez A, Deco G, Hagmann P, Romani GL, Mantini D, Corbetta M: Resting-state temporal synchronization networks emerge from connectivity topology and heterogeneity. PLoS Comput Biol 2015; 11:e1004100
22. Pisauro MA, Benucci A, Carandini M: Local and global contributions to hemodynamic activity in mouse cortex. J Neurophysiol 2016; 115:2931–6
23. Thompson GJ, Riedl V, Grimmer T, Drzezga A, Herman P, Hyder F: The whole-brain "global" signal from resting state fMRI as a potential biomarker of quantitative state changes in glucose metabolism. Brain Connect 2016; 6:435–47
24. Fogel S, Albouy G, King BR, Lungu O, Vien C, Bore A, Pinsard B, Benali H, Carrier J, Doyon J: Reactivation or transformation? Motor memory consolidation associated with cerebral activation time-locked to sleep spindles. PLoS One 2017; 12:e0174755
25. Vahdat S, Fogel S, Benali H, Doyon J: Network-wide reorganization of procedural memory during NREM sleep revealed by fMRI. Elife 2017; 6:pii:e24987
26. Huang Z, Liu X, Mashour GA, Hudetz AG: Timescales of intrinsic BOLD signal dynamics and functional connectivity in pharmacologic and neuropathologic states of unconsciousness. J Neurosci 2018; 38:2304–17
27. Huang Z, Zhang J, Wu J, Liu X, Xu J, Zhang J, Qin P, Dai R, Yang Z, Mao Y, Hudetz AG, Northoff G: Disrupted neural variability during propofol-induced sedation and unconsciousness. Hum Brain Mapp 2018; 39:4533–44
28. Huang Z, Dai R, Wu X, Yang Z, Liu D, Hu J, Gao L, Tang W, Mao Y, Jin Y, Wu X, Liu B, Zhang Y, Lu L, Laureys S, Weng X, Northoff G: The self and its resting state in consciousness: An investigation of the vegetative state. Hum Brain Mapp 2014; 35:1997–2008
29. Huang Z, Zhang J, Wu J, Qin P, Wu X, Wang Z, Dai R, Li Y, Liang W, Mao Y, Yang Z, Zhang J, Wolff A, Northoff G: Decoupled temporal variability and signal synchronization of spontaneous brain activity in loss of consciousness: An fMRI study in anesthesia. Neuroimage 2016; 124(Pt A):693–703
30. Giacino JT, Kalmar K, Whyte J: The JFK Coma Recovery Scale-Revised: Measurement characteristics and diagnostic utility. Arch Phys Med Rehabil 2004; 85:2020–9
31. Huang Z, Zhang J, Longtin A, Dumont G, Duncan NW, Pokorny J, Qin P, Dai R, Ferri F, Weng X, Northoff G: Is there a nonadditive interaction between spontaneous and evoked activity? Phase-dependence and its relation to the temporal structure of scale-free brain activity. Cereb Cortex 2017; 27:1037–59
32. He BJ: Scale-free properties of the functional magnetic resonance imaging signal during rest and task. J Neurosci 2011; 31:13786–95
33. Power JD, Barnes KA, Snyder AZ, Schlaggar BL, Petersen SE: Spurious but systematic correlations in functional connectivity MRI networks arise from subject motion. Neuroimage 2012; 59:2142–54
34. Power JD, Mitra A, Laumann TO, Snyder AZ, Schlaggar BL, Petersen SE: Methods to detect, characterize, and remove motion artifact in resting state fMRI. Neuroimage 2014; 84:320–41
35. Horovitz SG, Braun AR, Carr WS, Picchioni D, Balkin TJ, Fukunaga M, Duyn JH: Decoupling of the brain's default mode network during deep sleep. Proc Natl Acad Sci USA 2009; 106:11376–81
36. Power JD, Cohen AL, Nelson SM, Wig GS, Barnes KA, Church JA, Vogel AC, Laumann TO, Miezin FM, Schlaggar BL, Petersen SE: Functional network organization of the human brain. Neuron 2011; 72:665–78
37. Bennett MR, Farnell L, Gibson W, Lagopoulos J: On the origins of the 'global signal' determined by functional magnetic resonance imaging in the resting state. J Neural Eng 2016; 13:016012
38. Monti MM, Lutkenhoff ES, Rubinov M, Boveroux P, Vanhaudenhuyse A, Gosseries O, Bruno MA, Noirhomme Q, Boly M, Laureys S: Dynamic change of global and local information processing in propofol-induced loss and recovery of consciousness. PLoS Comput Biol 2013; 9:e1003271
39. Schröter MS, Spoormaker VI, Schorer A, Wohlschläger A, Czisch M, Kochs EF, Zimmer C, Hemmer B, Schneider G, Jordan D, Ilg R: Spatiotemporal reconfiguration of large-scale brain functional networks during propofol-induced loss of consciousness. J Neurosci 2012; 32:12832–40

40. Huang Z, Vlisides PE, Tarnal VC, Janke EL, Keefe KM, Collins MM, McKinney AM, Picton P, Harris RE, Mashour GA, Hudetz AG: Brain imaging reveals covert consciousness during behavioral unresponsiveness induced by propofol. Sci Rep 2018; 8:13195
41. Liang Z, King J, Zhang N: Intrinsic organization of the anesthetized brain. J Neurosci 2012; 32:10183–91
42. Hamilton C, MaY, Zhang N: Global reduction of information exchange during anesthetic-induced unconsciousness. Brain Struct Funct 2017; 222:3205–16
43. Mashour GA, Hudetz AG: Neural correlates of unconsciousness in large-scale brain networks. Trends Neurosci 2018; 41:150–60
44. Matsui T, Murakami T, Ohki K: Transient neuronal coactivations embedded in globally propagating waves underlie resting-state functional connectivity. Proc Natl Acad Sci USA 2016; 113:6556–61
45. Sanchez-Vives MV, McCormick DA: Cellular and network mechanisms of rhythmic recurrent activity in neocortex. Nat Neurosci 2000; 3:1027–34
46. Vyazovskiy VV, Olcese U, Hanlon EC, Nir Y, Cirelli C, Tononi G: Local sleep in awake rats. Nature 2011; 472:443–7
47. Brown EN, Lydic R, Schiff ND: General anesthesia, sleep, and coma. N Engl J Med 2010; 363:2638–50
48. Fang Z, Ray LB, Houldin E, Smith D, Owen AM, Fogel SM: Sleep spindle-dependent functional connectivity correlates with cognitive abilities. J Cogn Neurosci 2020; 32:446–66
49. Bayne T, Hohwy J, Owen AM: Are there levels of consciousness? Trends Cogn Sci 2016; 20:405–13